Biosensors and Bioelectronics 99 (2018) 375–381

Contents lists available at ScienceDirect

Biosensors and Bioelectronics

journal homepage: www.elsevier.com/locate/bios

para-Sulfonatocalix[4]arene stabilized gold nanoparticles multilayers interfaced to electrodes through host-guest interaction for sensitive ErbB2 detection

Xingxin Wang[a,1], Dongshu Du[b,1], Haibin Dong[a,c], Sunfengda Song[a], Kwangnak Koh[d,*], Hongxia Chen[a,*]

[a] *Laboratory of Biosensing Technology, School of Life Sciences, Shanghai University, Shanghai 200444, PR China*
[b] *School of Life Sciences, Shanghai University, Shanghai 200444, PR China*
[c] *Shanghai Key Laboratory of Bio-Energy Crops, School of Life Sciences, Shanghai University, Shanghai 200444, PR China*
[d] *Institute of General Education, Pusan National University, Busan 609-735, Republic of Korea*

ARTICLE INFO

Keywords:
Human epidermal growth factor receptor 2
Gold nanoparticles
Supramolecule
Electrode interface
Layer by layer

ABSTRACT

Nanoparticle (NP) structure, compositing and the nature of the NP-functionalized electrode interface have a strong influence upon electrochemical properties that are critical in applications such as sensing, photocatalysis and electrocatalysis. Existing methods to fabricate NP-functionalized electrodes do not allow or precise control over all these variables, especially the NP-electrode interface, making it difficult to understand and predict how structural changes influence electrode activity and consequently limit the application. To conquer this problem, in this study, we fabricated a stepwise construction of a novel supramolecular stabilized gold nanoparticles (AuNPs) multilayer mediated by guest molecules, yielding 3D AuNPs assembly at the electrode interface. *para*-Sulfonatocalix[4]arene (pSC_4), a water soluble macrocyclic synthetic receptor, has been served as a stabilizing ligand for preparation and gaining new insights into pSC_4 stabilized gold nanoparticles (pSC_4-AuNPs) tethered on the electrode interface through host-guest interaction. We investigated the electrochemical properties of multilayer pSC_4-AuNPs modified gold electrode using different core size of AuNPs with varying layer number. The electron transfer ability was characterized by electrochemical impedance spectroscopy (EIS). Electrochemical signals are significantly enhanced through the layer-by-layer assembly of pSC_4-AuNPs due to its high conductivity and high effective area. With this innovative method, by taking the assay of a tumor marker as an example, human epidermal growth factor receptor 2 (ErbB2) was successfully measured with a detection limit of 0.5 ng/mL. Taking the advantage of the pSC_4-AuNPs multilayer's good biocompatibility, high effective area and high electronic transmission, 3D AuNPs multilayer produced on the electrode interface suggests a portable synthetic pathway for the application into sensitive electrochemical biosensor.

1. Introduction

Gold nanoparticles (AuNPs) has important effect in the fields of nanotechnology and nanomaterials on account of their importance in biosensors (Siwy et al., 2005), nanoelectronics (Hassenkam et al., 2004; Zheng et al., 2011; He et al., 2017), catalysis (Chen and Goodman, 2008) and so on. Their good biocompatibility, high chemical stability, surface functionalization, and facile synthesis make them considerable building blocks for novel hybrid nanomaterials (Ofir et al., 2008; Klajn et al., 2010). Macrocycles, such as cyclodextrins, cucurbiturils, and calixarenes still remain major to supramolecular chemistry (Dsouza et al., 2011; Yang, 2011; Sun et al., 2012a). Lately, progress has been created in the synthesis and assembly of metal nanoparticles capped with cyclodextrins (Liu et al., 1999; Heo et al., 2012), cucurbiturils (Lee and Scherman, 2010, 2012), and calixarenes (Wei, 2006). Construction of AuNPs and supramolecular macrocycles expressively combines and enhances the features of the two entities (Crespo-Biel et al., 2005; Li et al., 2013), for instance the thermal, electronic, and catalytic properties of AuNPs and molecular recognition of the macrocyclic hosts, extending potential applications as biosensors (Sun et al., 2012b; Liu et al., 2005; Kim et al., 2010). Among them, several colorimetric and fluorescence sensors which combine the

* Corresponding authors.
E-mail addresses: koh@pusan.ac.kr (K. Koh), hxchen@shu.edu.cn (H. Chen).
[1] These authors contributed equally to this work.

http://dx.doi.org/10.1016/j.bios.2017.08.011
Received 19 June 2017; Received in revised form 31 July 2017; Accepted 7 August 2017
Available online 08 August 2017
0956-5663/

recognition function of supramolecular and SPR of AuNPs were reported recently (Lazar et al., 2016; Guo et al., 2013). However, these methods are suffering the higher detection limit and cannot be applied to the sensitive clinical requirement. Applying supramolecules modified AuNPs as sensors' interface can solve this problem. As an alternative technique to photometry, electrochemical approach potentially provides a more attractive method for biomarker assessment (De Leener et al., 2016). Electrochemical detection of noble metal ions (Wei et al., 2015), small bioactive molecules (Nguyen et al., 2010), DNA (Chakraborty et al., 2015), enzymes (Xianyu et al., 2015) and cancer marker proteins (Lu et al., 2015) have been reported with ultrahigh specificity and sensitivity. Electrochemical method also cost efficient and easier to miniaturize in a compact device, so it has received great interests (McWilliams et al., 2015).

Recently, the principle of nanoparticle-functionalized electrode has been reported to enhance the electrochemical properties that are critical in applications such as amperometric sensing, photocatalysis and electrocatalysis (Young et al., 2016). Unfortunately, disordered arrangement of NP on electrode has restricted enhancement of electrochemical properties. It cannot still get a stabilized functionalized film and make a slight signal enhancement. Young et al. (2016) found the molecular tethered AuNP-electrode interface results in more efficient electron transfer than solution deposited samples. Therefore, in comparison with one layer molecular tethered AuNP electrode interface, self-assembled multi-AuNP layers can be adapted to fabricate more efficient electrochemical activity interface in several aspects. First, conductivity in 3D assemblies of AuNPs can increase comparing with 2D AuNP. Wessels et al. characterize the optical and electrical properties of three-dimensional interlinked AuNPs assemblies (Wessels et al., 2004; Midtvedt et al., 2016). They present linker molecules that enable tuning of the conductivity in 3D assemblies of AuNPs from the semiconducting to the metallic limit by varying the degree of conjugation of the linker molecule and the nature of its metal binding groups. Second, 3D assemblies of AuNPs can be constructed through the self-assembled NP multilayers based on host-guest interaction. Crespo-Biel et al. developed the stepwise construction of a self-assembled organic/inorganic multilayers based on multivalent supramolecular interactions between guest-functionalized dendrimers and host-modified AuNPs, yielding a controlled supramolecualr layer-by-layer assembly (Crespo-Biel et al., 2005; Lu et al., 2016). Third, calixarene derivatives have been confirmed as proteins' linker by binding the amine groups of proteins' through several noncovalent soft bindings (Chen et al., 2010). Additionally, increasing amounts of AuNPs are gathered onto the electrode surface, which significantly amplifies the amount of probe proteins. On the basis of the four aforementioned aspects, a general method is first put forward for convert self-assemble multilayer of supramolecular-AuNP into a more sensitive surface-tethered electrochemical analysis interface.

Here, we represent the stepwise construction of a novel kind of self-assembled supramolecular functionalized AuNPs (pSC_4-AuNPs) multilayers based on supramolecular host-guest interactions between guest molecules and host-modified nanoparticles. Such protocols can potentially be used for obtaining particular structures, whose assembly is determined by multiple supramolecular interactions (Li et al., 2013). The ultimate tridimensional control, when combined with top-down surface patterning strategies such as monomolecular film for surface control, can lead to 3D nanofabrication schemes.

Human epidermal growth factor receptor 2 (ErbB2 or HER2) is a tyrosine kinase receptor vesting in the epidermal growth factor receptor (EGFR) family and is related to cellular signaling pathways, which result in cell proliferation, growth, apoptosis and differentiation (Özcelik et al., 2002). These processes are vital to life, but loss function of control within these pathways is continually tied to several diseases, including cancer (Harari and Yarden, 2000). As the overexpression of ErbB2 is observed in some of breast cancer conditions (thus cataloged as ErbB2 positive) and therapies using a monoclonal antibody to this molecule is present in use, it is only valid in patients with excess receptor levels (Negro et al., 2006). As it is, it is requested to screen the patients before therapy to find those who are qualified for such administrations. The blood ErbB2 content of breast cancer patients is generally > 0.015 μg/mL, which demands assay methods competent to undoubtedly measure such low concentration levels in this sophisticated biological sample (Martin et al., 2006). Current diagnostic tests for ErbB2 comprise the use of immunohistochemistry (IHC) or fluorescent in situ hybridization (FISH), which are optical semi-quantitative techniques (Jiang et al., 2008; Portier et al., 2013). Additionally, both procedures are detailed and time consuming, demand exhaustive sample preparations and desire specially trained personnel to perform the corresponding multi-step procedure (Kallioniemi et al., 1992; Ouyang et al., 1999). In this work, we have fabricated a simple and efficient, label-free and highly sensitive electrochemical method for ErbB2 detection. As presented in Scheme 1, a supramolecule *para*-sulfonatocalix[4]arene (pSC_4) with a pore size of 3.8 Å is employed in this work as the substrate (Shinkai et al., 1988). After being covalently modified onto the gold electrode surface, pSC_4 was used here to play a role of the substrate layer from forming host-guest interaction. The 1,6-hexanediamine (HMD) solution was then added to react with pSC_4 through host-guest recognition for specific binding. The HMD and pSC_4-gold nanoparticles (pSC_4-AuNPs) were added one by one to assemble a layer-by-layer thin film. Electrochemical impedance spectroscopy (EIS) was used investigated the electrochemical properties of multilayer pSC_4-AuNPs modified gold electrode using different core size of AuNPs with varying layer number. Electrochemical signals are significantly improved through the layer-by-layer assembly of pSC_4-AuNPs. Own to the pSC_4-AuNPs multilayer's good biocompatibility and high electronic transmission, ErbB2 was quantified with a concentration range from 0.001 μg/mL to 10 μg/mL. The signal amplification is a novel label-free detection concept for the design of highly sensitive analytical methods for the detection of biomarker.

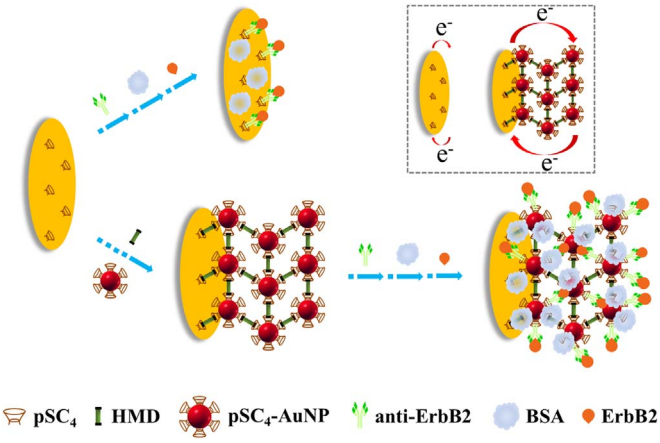

Scheme 1. Schematic of pSC_4 monolayer and pSC_4-AuNPs layer-by-layer signal amplification on the electrode surface.

2. Experimental section

2.1. Materials and apparatus

Human ErbB2/HER2 protein (10004-HCCH) and its mouse monoclonal antibodies (10004-MM03) were purchased from Sino Biological (Beijing, China). Hydrogen tetrachloroaurate trihydrate ($HAuCl_4 \cdot 3H_2O$) was purchased from Sigma-Aldrich, Inc. (St. Louis, USA). Sodium borohydride was purchased from Aladdin, Inc. (Shanghai, China). Bovine serum albumin, vascular endothelial growth factor and 1,6-hexanediamine were purchased from Sinopharm Chemical Reagent Co., Ltd. (Shanghai, China). *para*-Sulfonatocalix[4]arene was purchased from TCI (Shanghai) Development Co., Ltd. (Shanghai,

China). All other chemical reagents were analytical grade. All solutions were prepared with deionized water purified with a Milli-Q purification system (Branstead, USA) to a specific resistance of 18 MΩ cm.

The UV–vis spectra were obtained by a Shimadzu UV-2450 PC UV–vis spectrophotometer, with a quartz cuvette having a volume of 50 µL and a path length of 10 mm. TEM was recorded on a JEM-2010F instrument with an operating accelerating voltage of 200 kV. The surface modification was monitored by Fourier-transform infrared (FT-IR) spectroscopy (JASCO, FTIR6300, Japan). The sample was centrifuged twice, drop-casted on a carbon coated copper grid, and dried under an infrared lamp. The zeta-potential data was acquired with a Malvin Zetasizer 3000HS system. SPR was conducted with an Autolab ESPRIT system (Eco Chemie B.V., the Netherlands). The electrochemical measurements were conducted with an Autolab PGSTAT128N system (Eco Chemie B.V., the Netherlands).

2.2. Synthesis of the pSC_4-AuNPs

In order to compare the size effect on proposed system, two different sizes of pSC_4-AuNPs were synthesized. In case of bigger size NPs (Han et al., 2009), pSC_4 (2 mL, 10^{-2} mol/L) and $HAuCl_4$ solutions (2 mL, 2.63×10^{-2} mol/L) were added to 94 mL of water in turn at room temperature. After stirring for 20 min in the dark, freshly prepared $NaBH_4$ solution (2 mL, 10^{-2} mol/L) was added into the reaction solution immediately, and then continues stirring for 2 h in the dark. A procedural colour change from bright yellow to light brown and brownish red was observed. The pSC_4-AuNP colloids were finally obtained. Small size pSC_4-AuNPs was synthesized according to previous methods (Masitas et al., 2016). The whole process of synthesis of small size pSC_4-AuNPs is similar to bigger size pSC_4-AuNPs. The difference amount of substances are added to obtain small size pSC_4-AuNPs as following: pSC_4 (2 mL, 2×10^{-3} mol/L), $HAuCl_4$ solutions (2 mL, 1.25×10^{-3} mol/L), 96 mL of water and $NaBH_4$ solution (2 mL, 2×10^{-3} mol/L). The resulting solution was light red and stored at 4 °C in an amber bottle and ready for use. UV–vis spectra, zeta-potential, TEM and FT-IR were used to characterize the prepared AuNPs.

2.3. Immobilization of pSC_4 on the gold chip surface

The bare gold chip was first immersed in piranha solution (98% H_2SO_4: 30% H_2O_2 = 3:1) for 5 min to eliminate the modified material and then rinsed with DW. The prepared gold chip was fixed on the SPR instrument. After that, pSC_4 was immobilized on the gold chip through $Au–SO_3^-$ bond at 25 °C for overnight via incubation with a 10 mM pSC_4 solution as previously described (Han et al., 2009). Behind the immobilization, the gold chip was rinsed with DW. The immobilization process was monitored via SPR spectroscopy.

After rinsing with DW, the pSC_4-treated gold chip was immersed into 100 µL of HMD solution for 20 min. Then, the gold chip was flushed with DW to remove the unconjugated HMD until a stable SPR baseline was acquired. A 100 µL aliquot of pSC_4-AuNP solution was then added to react with HMD through host-guest recognition due to specific binding. The gold chip was rinsed with DW to remove unbound pSC_4-AuNPs. Finally, the HMD and pSC_4-AuNPs were added one by one to fabricate a layer-by-layer signal amplification (Li et al., 2013). The total process was monitored via SPR spectroscopy in real time at 25 °C (± 0.3).

2.4. Electrode preparation and modification

The gold electrode (3.0 mm diameter) was firstly purified with piranha solution (98% H_2SO_4: 30% H_2O_2 = 3:1) for 5 min to eliminate the modified material and then rinsed with DW. After that, the electrode was polished discreetly with 1, 0.3 and 0.05 µm alumina slurry, respectively. The residual alumina powder was removed by sonicating the electrode unceasingly in both ethanol and DW sequentially. Subsequently, the electrode was operated electrochemically to remove any remaining impurities with 0.5 M H_2SO_4. Lastly, the electrode was dried by purging with nitrogen.

To prepare pSC_4-AuNPs with substrate gold electrode, the gold electrode was firstly incubated with 100 µL of 10 mM pSC_4 solution for overnight at 25 °C. pSC_4 was used here to play a role of the substrate layer from forming host-guest interaction. The remaining pSC_4 was removed by rinsing thoroughly with the washing buffer for 3 times. The pSC_4-modified gold electrode was then immersed in 100 µL of HMD solution (1 mM) for 20 min to construct the well-aligned pSC_4-AuNPs layers.

2.5. Fabrication of ErbB2 biosensor and electrochemistry detection

ErbB2/HER2 antibody was used as a recognition molecule and immobilized onto the modified gold electrode. The gold electrode was incubated in the ErbB2 antibody solution (10 µg/mL) for 1 h. After rinsing with DW, the ErbB2 antibody treated electrode was immediately immersed into 100 µL BSA solutions (0.1 mg/mL) for 30 min. The treated gold electrode was then immersed in 100 µL of ErbB2 solution (0.001, 0.01, 0.1, 1 and 10 µg/mL) for 30 min, followed by washing with DW. The entire process was performed at room temperature.

2.6. Electrochemical measurements

The electrochemical measurements by using electrochemical impedance spectroscopy (EIS) were performed on a model Autolab PGSTAT128N system with a conventional three-electrode cell at room temperature. A platinum wire electrode as the counter electrode, and a saturated calomel electrode (SCE) was used as the reference electrode.

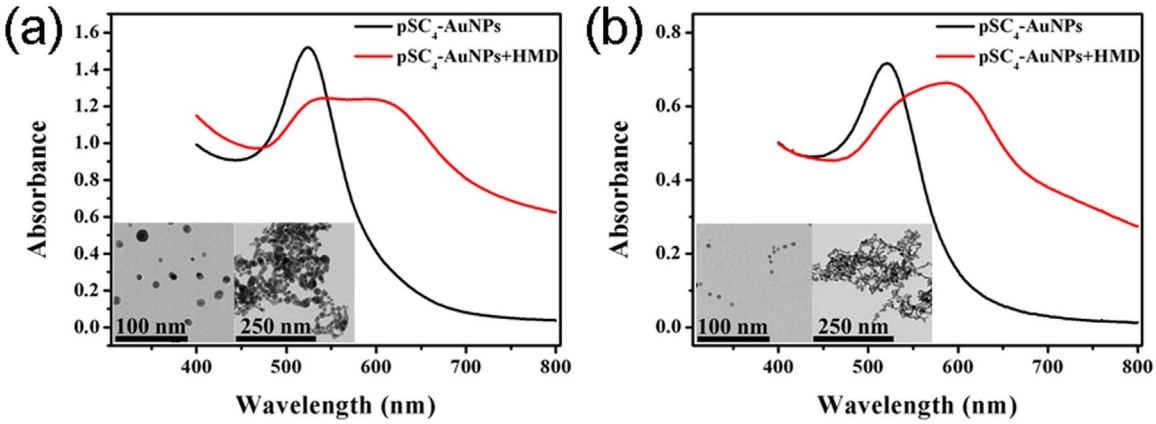

Fig. 1. UV–vis spectra of pSC_4-AuNPs before (black trace) and after in the presence of HMD (red trace) for 16 nm pSC_4-AuNPs (a) and 4 nm pSC_4-AuNPs (b). Inserts, TEM images of pSC_4-AuNPs before (left) and after in the presence of HMD (right).

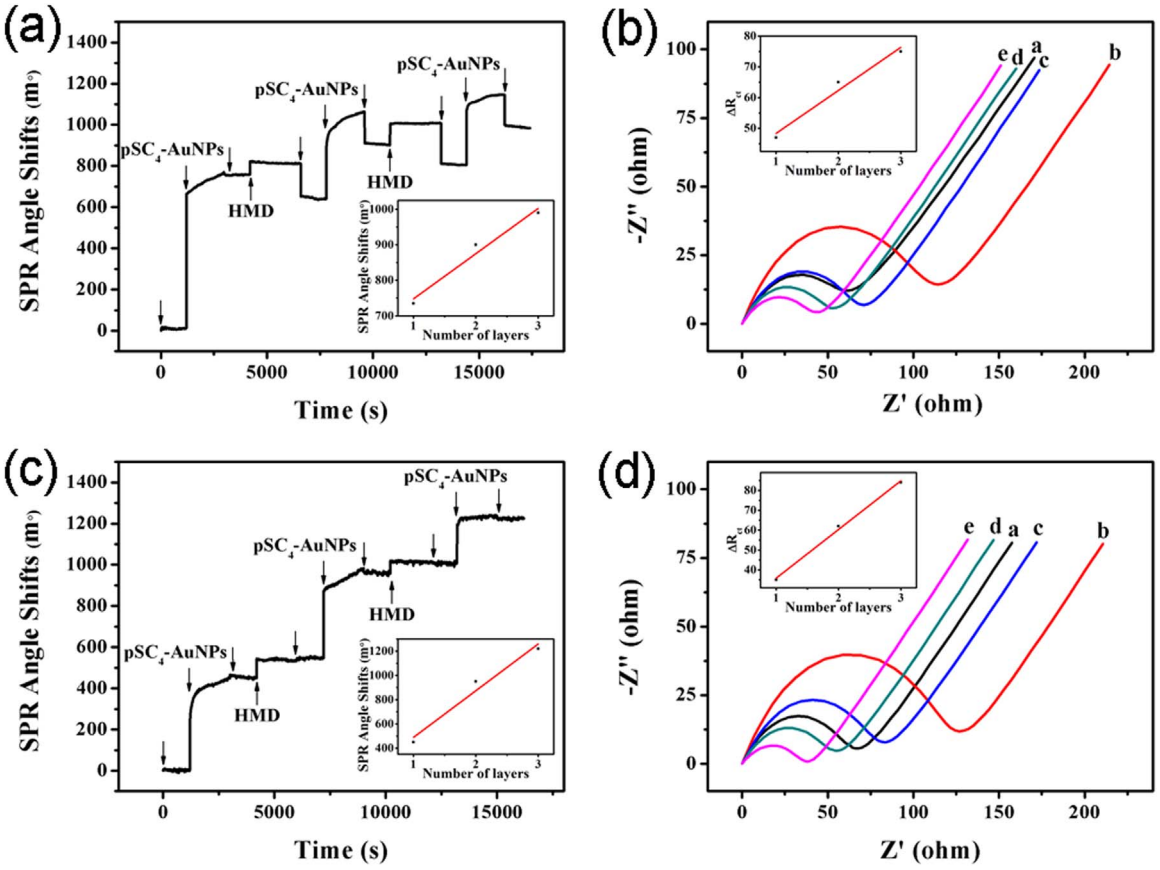

Fig. 2. Sensorgram of SPR angle shifts and EIS according to the assembly process of HMD and pSC_4-AuNPs on the chip surface (a, b for 16 nm pSC_4-AuNPs and c, d for 4 nm pSC_4-AuNPs respectively). (b) and (d): curves a to e represent bare gold electrode, pSC_4 modified gold electrode, 1 layer pSC_4-AuNPs on pSC_4 modified gold electrode, 2 layers pSC_4-AuNPs on pSC_4 modified gold electrode and 3 layers pSC_4-AuNPs on pSC_4 modified gold electrode respectively. Insert: SPR and EIS changes as a function of the number of bilayer of HMD and pSC_4-AuNPs on pSC_4 modified gold surface.

EIS data was performed within the frequency range from 0.1 Hz to 100 kHz and the amplitude was 5 mV, and the direct current potential was fettered at the formal potential of the redox pair $[Fe(CN)_6]^{3-/4-}$ (0.224 V versus SCE). The electrolyte solution for EIS measurements was 5 mM $K_3[Fe(CN)_6]/K_4[Fe(CN)_6]$ solution embracing 0.1 M KCl.

3. Results and discussion

3.1. Characterization of pSC_4-AuNPs

In order to study the AuNPs core size effect, two different sizes of pSC_4-AuNPs were synthesized by reducing $HAuCl_4$ with in the presence of the selected concentrations of pSC_4. Corresponding UV–vis spectra are shown in Fig. 1. The well-known SPR of AuNPs was observed at 524 nm and 517 nm respectively, suggesting the formation of stable and different size of pSC_4-AuNPs. The Fig. 1 inserts show the TEM images of as prepared pSC_4-AuNPs with a size of 16 and 4 nm respectively. Big size of pSC_4-AuNPs were characterized by zeta-potential with a mean size of 16 nm and − 37.3 mV in potential to verify its stability and good dispersity as shown in Fig. S1a and b, which are consistent with the results of UV–vis spectra. All these data confirmed that pSC_4-AuNPs is stable and in good disperse. FT-IR spectroscopy was used to monitor whether AuNPs were indeed capped by pSC_4. Fig. S1c shows the FT-IR spectra of pure pSC_4 and AuNPs

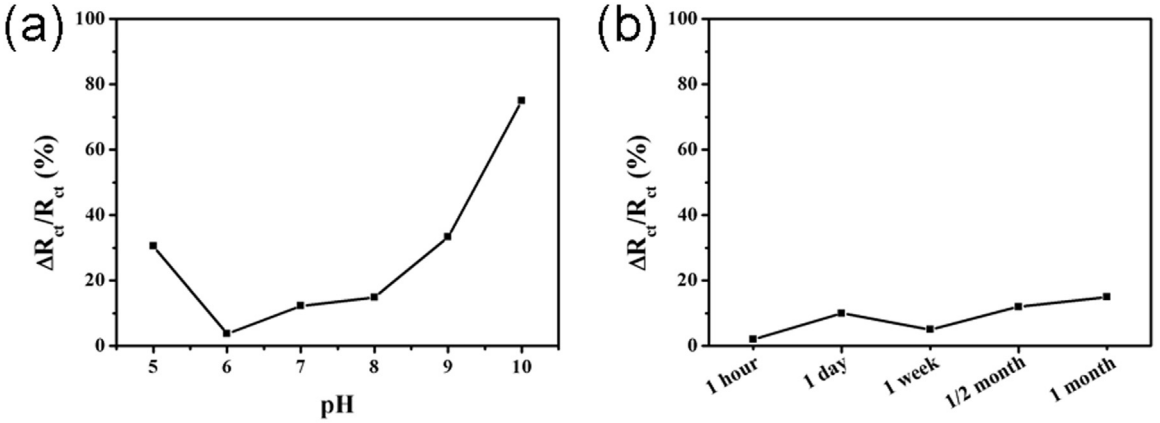

Fig. 3. Stability of electrochemical biosensor at different pH conditions (a) and different time conditions (b).

modified with pSC_4. Comparing the FT-IR spectra of pSC_4 and pSC_4-AuNPs, significant features can be seen: the peaks for SO_3^- at 1187 cm^{-1} and 1049 cm^{-1}, as found in pure pSC_4, are shifted to 1178 cm^{-1} and 1035 cm^{-1}, respectively, which suggests that the SO_3^- groups coordinate with the Au atoms on the surface of the AuNPs (Han et al., 2009).

To prove the principle of the detection system, the host-guest recognition between HMD and pSC_4-AuNPs was also measured by UV–vis spectroscopy. After mixing HMD and pSC_4-AuNPs, the peak at 524 nm and 517 nm decreases, and a new peak at 625 nm and 608 nm appear for big and small pSC_4-AuNPs respectively (Wu et al., 2017). These peaks reveal that an interaction exists between HMD and pSC_4-AuNPs. In order to study the HMD-controlled self-assembly of pSC_4-AuNPs, pSC_4-AuNPs samples before and after addition of HMD were characterized by transmission electron microscopy (TEM) (Fig. 1, insert). The as-synthesized pSC_4-AuNPs have a relatively narrow size distribution with the average diameter around 16 nm and 4 nm respectively. According to the obvious behaviour of the pSC_4-AuNPs in the absence and presence of HMD, pSC_4 on the surface of AuNPs can interact with HMD, resulting in distinct aggregation of the pSC_4-AuNPs. These results demonstrate that pSC_4-AuNPs were synthesized successfully and are ready for the next signal accumulation.

3.2. Building multilayer thin film on gold chip surface

SPR and EIS were used to monitor the supramolecular assembly of pSC_4-AuNPs and HMD on gold surface (Fig. 2). pSC_4 was immobilized on the gold chip surface firstly through self-assembly via the covalent bond between Au and the SO_3^- group of pSC_4 as described elsewhere (Han et al., 2009). pSC_4 prefers to bind in high affinity and specificity to N-terminal HMD. Then, pSC_4-AuNPs combined with electrode surface through HMD. In order to study the size effect, two kinds of AuNPs were utilized to fabricate the 3D AuNP layers with a diameter of 16 nm and 4 nm respectively. As shown in Fig. 2a and c, the SPR angle shifted evidently with the layer-by-layer conjugation of HMD and pSC_4-AuNPs in both cases. After the first cycle of HMD and pSC_4-AuNP conjugation, the SPR angle shifts by 735 and 400 millidegree for big and small size of AuNPs, respectively. The second and third cycles of HMD and pSC_4-AuNP conjugation of SPR angle shifts were 400 and 200 millidegrees for big size, respectively. In case of small size of AuNPs, the second and third cycles of HMD and pSC_4-AuNP conjugation of SPR angle shifts were 600 and 200 millidegrees. The total SPR increase is similar for both sizes of AuNPs. These findings reveal the successful conjugation of HMD and pSC_4-AuNPs onto the surface of the gold chip layer-by-layer, which can be further verified by EIS. As shown in Fig. 2b and d, the evident decrease in interfacial electron resistance with the layer-by-layer conjugation of HMD and pSC_4-AuNPs on the gold electrode surface can be ascribed to the high electronic transmission of pSC_4-AuNPs between the gold electrode and $[Fe(CN)_6]^{3-/4-}$ (Wei et al., 2015; Young et al., 2016). EIS data are fitted to an Equivalent Electrical Circuit (EEC) to extract quantitative information about the processes occurring at the surface of the electrode (Fig. S2). pSC_4-AuNPs have been utilized for this process and envisioned that HMD could bridge pSC_4-modified AuNPs together to achieve patterned AuNPs. Indeed, when HMD was added, one-dimensional (1D) chain-like and three-dimensional network-like self-assembled architectures, rather than simply mass aggregation were observed. Further characterization of the multilayer films was performed by means of EIS (Fig. 2b and d). A similar trend during the fabrication of the multilayer on the electrode surface was observed in both cases. After the pSC_4-AuNPs were composited with the gold electrode layer by layer through the host-guest interaction, the R_{ct} value was decreased, which confirmed the significant facilitate the interface on NP-mediated electron transfer and suggests the multilayer pSC_4-AuNPs film modified electrodes can serve as versatile platforms for applications of sensitive biosensor platform.

Fig. 2 inserts show a linear decrease in R_{ct} and SPR angle shifts increase with the number of layers, which confirms our method allows and can precise controlled over especially the NP-electrode interface, making it possible to understand how structural changes influence electrode activity for further sensitive biosensor application. The electric properties of two size AuNP multilayer modified gold electrode are similar. These SPR and EIS spectra were depicted a successful network AuNPs on the gold surface for both sizes AuNPs. Therefore, for easy synthesis and characterization, 16 nm AuNPs were selected for next detection.

Furthermore, it is found that the obtained pSC_4-AuNPs multilayer thin film has the good stability. Fig. 3a exhibits the pH dependent curve

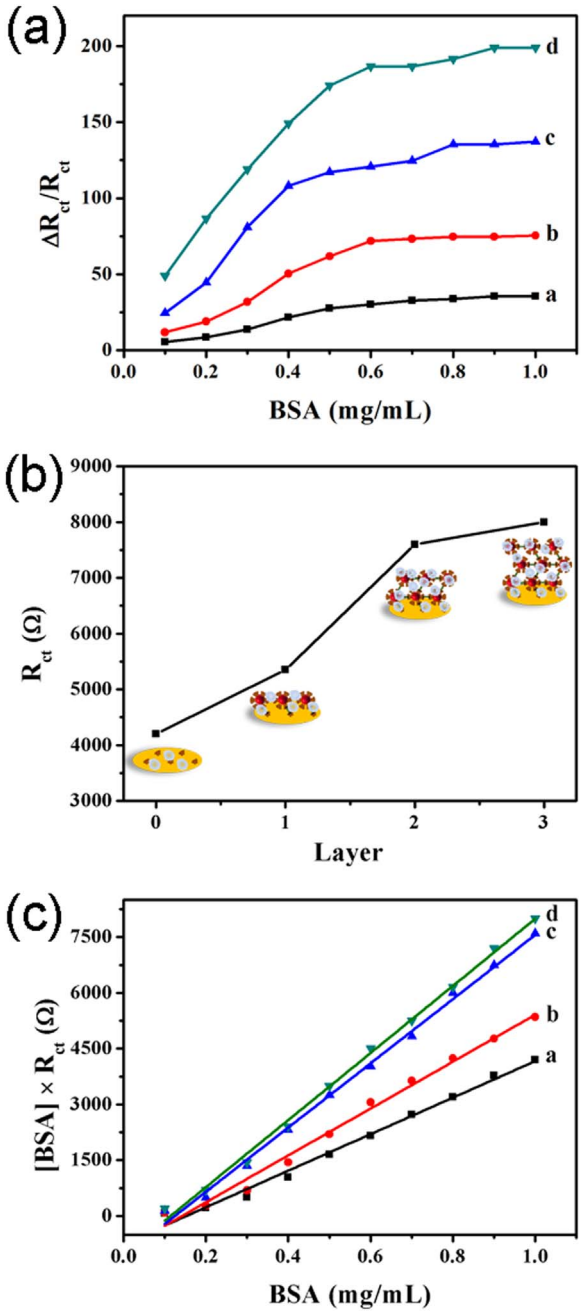

Fig. 4. (a) Curve a–d means pSC_4 and different layers (1–3) of HMD and pSC_4-AuNPs-modified electrode after treatment with BSA solution 30 min for 0.1, 0.2, 0.3, 0.4, 0.5, 0.6, 0.7, 0.8, 0.9 and 1.0 mg/mL respectively. Test solution: 5 mM $[Fe(CN)_6]^{3-/4-}$ and 0.1 M KCl. (b) Relationship between the electrode resistance change and the layer number of pSC_4-AuNPs. (c) The linear relationship between the $c{\cdot}R_{ct}$ and the concentration of BSA.

via EIS difference of pSC_4-AuNPs multilayer response to different pH. The results indicate that the pSC_4-AuNPs multilayer remained stable during a pH value of 6–8. Fig. 3b shows the EIS difference of pSC_4-AuNPs multilayer corresponding to the different times. The pSC_4-AuNPs multilayers are stable enough after storage of 1 month, only a slight drop of R_{ct} can be observed.

3.3. Protein adsorption on the multilayer thin film

The amount of the protein on the sensor surface should be concerned in order to make a sensitive biosensor. BSA was utilized a model protein to study the protein adsorption on the pSC_4-AuNPs multilayer thin film modified interface. Different layers of HMD and pSC_4-AuNPs involved in the detection were compared to optimize the sensing condition. First, the commonly used EIS was employed to characterize the adsorption efficiency of the different layers conjugation of HMD and pSC_4-AuNPs at pSC_4-modified gold electrode. Fig. 4a shows the EIS record for the pSC_4-modified gold electrode immersed in a BSA solution for different concentrations, respectively. The electron resistance obviously increases because BSA can be absorbed by the layer conjugation of HMD and pSC_4-AuNPs on the chip surface. These results reveal that the adsorption reaction is completed within the BSA concentration of 1.0 mg/mL. Second, BSA adsorption at different layer of pSC_4-AuNPs was measured on the basis of EIS (Fig. 4a). The amount of BSA is increased according to the layer increasing and shows no apparent increase at 3 layers (Fig. 4b). The relationship between the concentrations of the protein at the multilayer surface as a function of its solution concentration is described by the adsorption isotherm. The shape of the isotherm shows a knee and then exhibits a transition to a plateau (Fig. 4a). This type of isotherm can be described by the Langmuir model using the equation (Kresak et al., 1977):

$$\Gamma = \frac{B_{ADS}\Gamma_{\max}C}{1 + B_{ADS}C} \quad (1)$$

where Γ_{max} is the maximum number of adsorption sites per unit of surface area (mol/m^2) of adsorbent and B_{ADS} is the affinity of the adsorbent molecules (L/mol) for the adsorption sites. Because the $1/R_{ct}$ is directly proportional to R_{ct}, the upper form is rewritten as:

$$cR_{ct} = \frac{1}{B_{ADS}}R_{ct(\max)} + cR_{ct(\max)} \quad (2)$$

The linearized form of the isotherm is a plot of cR_{ct} vs. c as shown in Fig. 4c. The correlation coefficient (r) is equal to 0.988, 0.989, 0.996 and 0.996 for line a to d, respectively. The adsorption of BSA on pSC_4-AuNPs multilayer thin film surface was basically consistent with Langmuir. The adsorption isotherm is absorbed by single molecule layer. The total adsorption amount of BSA on the 3 layer of pSC_4-AuNPs surface is 5 times than that of bare gold surface. Therefore, for the handling convenient and sensor's best property, 3 layers were selected in next sensitivity measurement.

3.4. Sensor's sensitivity and selectivity

The EIS detection of ErbB2 was performed to assess the sensing strategy with the HMD and pSC_4-AuNPs as amplification reagents under optimized experiment conditions. As shown in Fig. 5a, the electron-transfer resistance gradually increase as the concentration of ErbB2 increases from 0.001 μg/mL to 10 μg/mL because of antibody-

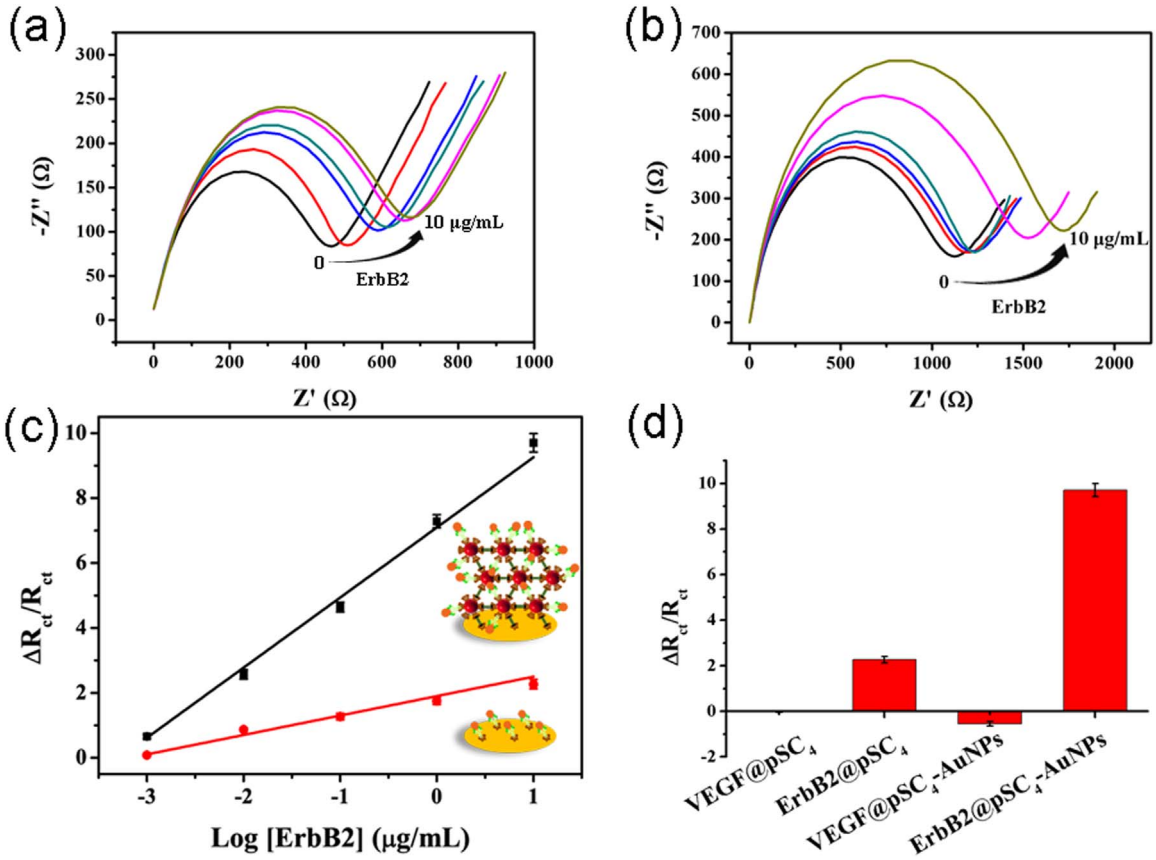

Fig. 5. (a) Electrode resistance sensorgrams for the direct detection of ErbB2 at 0.001, 0.01, 0.1, 1 and 10 μg/mL. Test solution: 5 mM $[Fe(CN)_6]^{3-/4-}$ and 0.1 M KCl. (b) Electrode resistance sensorgrams for the amplified detection of ErbB2 at 0.001, 0.01, 0.1, 1 and 10 μg/mL. Test solution: 5 mM $[Fe(CN)_6]^{3-/4-}$ and 0.1 M KCl. (c) Electrode resistance responses of the assay for different concentrations: 0.001, 0.01, 0.1, 1 and 10 μg/mL. (d) Electrode resistance responses of the assay for different proteins: 40 μg/mL VEGF with pSC_4 modified gold electrode, 10 μg/mL ErbB2 with pSC_4 modified gold electrode, 40 μg/mL VEGF with pSC_4-AuNPs modified gold electrode, and 10 μg/mL ErbB2 with pSC_4-AuNPs modified gold electrode. Error bars represent standard deviations of measurements (n = 3).

antigen interaction. The regression equation of $\Delta R_{ct}/R_{ct}$ = 2.1599C + 7.09558 (R^2 = 0.994). Eletxigerra et al. (2016) reported the detection of ErbB2 based on surface plasmon resonance with a LOD of 3.8 ng/mL, which relies on the differential binding of signal enhancement AuNP to a SPR chip surface. However, multiple steps by adding AuNP as a signal enhancement reporter will make the detection system more complex. With our method, the detection limit has been calculated to be 0.5 ng/mL by the interpolation of the mean plus three times the standard deviation of the zero standards. The obtained signals were enlarged about 10 times comparing with the electrode without pSC_4-AuNPs multilayer modification, which own to larger surface area to volume ratio and higher conductivity of 3D configurations of the nanostructures (Basu and Roy Chaudhuri, 2016).

Vascular endothelial growth factor (VEGF) and ErbB2 have been considered as potential therapeutic targets in cholangiocarcinoma (Yoshikawa et al., 2008). To evaluate the specificity of the detection method, VEGF was explored to evaluate the specificity of the electrochemical biosensor. As shown in Figs. 5d and S3, the electrochemical signal for 10 μg/mL ErbB2 remarkably increases compared with that for the VEGF (40 μg/mL) in both cases. However, the obtained ErbB2 selectivity signals were enlarged comparing with the electrode without pSC_4-AuNPs multilayer modification, which own to larger surface area to volume ratio and higher conductivity of 3D configurations of the nanostructures. These results manifest that the fabricated ErbB2 sensor displays a high selectivity.

4. Conclusions

pSC_4-modified AuNPs were successfully synthesized in aqueous solution, where pSC_4 with four sulfonate groups on each rim served for stabilizers. The interactions and assembly between guest molecules and pSC_4-modified AuNPs have also been researched and demonstrated. The stepwise construction of a novel kind of self-assembled multilayers is based on host-guest regulate pSC_4-AuNPs, which was confirmed with high stability and broad pH adaptable. pSC_4 on the surface of AuNPs served as amicable protein linker. Own to the increased amount of probe protein and the high electronic transmission of 3D multilayer pSC_4-AuNPs modified electrode interface, the sensitive and selectivity of sensors are dramatically improved. We anticipate that 3D multilayer pSC_4-AuNPs modified electrode can be used as sensitive electrochemical biosensor platform toward enhanced layer for ultrasensitive biomarker detection.

Acknowledgement

This work was supported by the National Natural Science Foundation of China (Grant No. 61275085).

Appendix A. Supplementary material

Supplementary data associated with this article can be found in the online version at http://dx.doi.org/10.1016/j.bios.2017.08.011.

References

Basu, J., RoyChaudhuri, C., 2016. IEEE Electron. Device Lett. 37, 492–495.
Chakraborty, S., Babanova, S., Rocha, R.C., Desireddy, A., Artyushkova, K., Boncella, A.E., Atanassov, P., Martinez, J.S., 2015. J. Am. Chem. Soc. 137, 11678–11687.
Chen, H., Huang, J., Lee, J., Hwang, S., Koh, K., 2010. Sens. Actuators B: Chem. 147, 548–553.
Chen, M., Goodman, D.W., 2008. Chem. Soc. Rev. 37, 1860–1870.
Crespo-Biel, O., Dordi, B., Reinhoudt, D.N., Huskens, J., 2005. J. Am. Chem. Soc. 127, 7594–7600.
De Leener, G., Evoung-Evoung, F., Lascaux, A., Mertens, J., Porras-Gutierrez, A.G., Le Poul, N., Lagrost, C., Over, D., Leroux, Y.R., Reniers, F., Hapiot, P., Le Mest, Y., Jabin, I., Reinaud, O., 2016. J. Am. Chem. Soc. 138, 12841–12853.
Dsouza, R.N., Pischel, U., Nau, W.M., 2011. Chem. Rev. 111, 7941–7980.
Eletxigerra, U., Martinez-Perdiguero, J., Barderas, R., Pingarrón, J.M., Campuzano, S., Merino, S., 2016. Anal. Chim. Acta 905, 156–162.
Guo, D.-S., Yang, J., Liu, Y., 2013. Chem. Eur. J. 19, 8755–8759.
Han, C., Zeng, L., Li, H., Xie, G., 2009. Sens. Actuators B: Chem. 137, 704–709.
Harari, D., Yarden, Y., 2000. Oncogene 19, 6102–6114.
Hassenkam, T., Moth-Poulsen, K., Stuhr-Hansen, N., Nørgaard, K., Kabir, M.S., Bjørnholm, T., 2004. Nano Lett. 4, 19–22.
He, L., Duan, F., Song, Y., Guo, C., Zhao, H., Tian, J.-Y., Zhang, Z., Liu, C.-S., Zhang, X., Wang, P., Du, M., Fang, S.-M., 2017. 2D Mater. 4, 025098.
Heo, D.N., Yang, D.H., Moon, H.-J., Lee, J.B., Bae, M.S., Lee, S.C., Lee, W.J., Sun, I.-C., Kwon, I.K., 2012. Biomaterials 33, 856–866.
Jiang, W., Kim, B.Y.S., Rutka, J.T., Chan, W.C.W., 2008. Nat. Nanotechnol. 3, 145–150.
Kallioniemi, O.-P., Kallioniemi, A., Kurisu, W., Thor, A., Chen, L.-C., Smith, H.S., Waldman, F.M., Pinkel, D., Gray, J.W., 1992. Proc. Natl. Acad. Sci. USA 89, 5321–5325.
Kim, C., Agasti, S.S., Zhu, Z., Isaacs, L., Rotello, V.M., 2010. Nat. Chem. 2, 962–966.
Klajn, R., Stoddart, J.F., Grzybowski, B.A., 2010. Chem. Soc. Rev. 39, 2203–2222.
Kresak, M., Moreno, E.C., Zahradnik, R.T., Hay, D.I., 1977. J. Colloid Interface Sci. 59, 283–292.
Lazar, A.I., Biedermann, F., Mustafina, K.R., Assaf, K.I., Hennig, A., Nau, W.M., 2016. J. Am. Chem. Soc. 138, 13022–13029.
Lee, T.-C., Scherman, O.A., 2010. Chem. Commun. 46, 2438–2440.
Lee, T.-C., Scherman, O.A., 2012. Chem. Eur. J. 18, 1628–1633.
Li, H., Chen, D.-X., Sun, Y.-L., Zheng, Y.B., Tan, L.-L., Weiss, P.S., Yang, Y.-W., 2013. J. Am. Chem. Soc. 135, 1570–1576.
Liu, J., Mendoza, S., Román, E., Lynn, M.J., Xu, R.L., Kaifer, A.E., 1999. J. Am. Chem. Soc. 121, (4304–4035).
Liu, Y., Yang, Y.-W., Chen, Y., 2005. Chem. Commun. 33, 4208–4210.
Lu, N., Gao, A., Dai, P., Mao, H., Zuo, X., Fan, C., Wang, Y., Li, T., 2015. Anal. Chem. 87, 11203–11208.
Lu, S.C., Mohamed, M., Zhu, W., 2016. 2D Mater. 3, 011010.
Martin, V.S., Sullivan, B.A., Walker, K., Hawk, H., Sullivan, B.P., Noe, L.J., 2006. Appl. Spectrosc. 60, 994–1003.
Masitas, R.A., Allen, S.L., Zamborini, F.P., 2016. J. Am. Chem. Soc. 138, 15295–15298.
McWilliams, M.A., Bhui, R., Taylor, D.W., Slinker, J.D., 2015. J. Am. Chem. Soc. 137, 11150–11155.
Midtvedt, D., Lewenkopf, C.H., Croy, A., 2016. 2D Mater. 3, 011005.
Negro, A., Brar, B.K., Gu, Y., Peterson, K.L., Vale, W., Lee, K.-F., 2006. Proc. Natl. Acad. Sci. USA 103, 15889–15893.
Nguyen, H.D., Dang, D.T., van Dongen, J.L.J., Brunsveld, L., 2010. Angew. Chem. Int. Ed. 49, 895–898.
Ofir, Y., Samanta, B., Rotello, V.M., 2008. Chem. Soc. Rev. 37, 1814–1825.
Ouyang, X., Gulliford, T., Doherty, A., Huang, G.C., Epstein, R.J., 1999. Lancet 353, 1591–1592.
Özcelik, C., Erdmann, B., Pilz, B., Wettschureck, N., Britsch, S., Hübner, N., Chien, K.R., Birchmeier, C., Garratt, A.N., 2002. Proc. Natl. Acad. Sci. USA 99, 8880–8885.
Portier, B.P., Wang, Z., Downs-Kelly, E., Rowe, J.J., Patil, D., Lanigan, C., Budd, G.T., Hicks, D.G., Rimm, D.L., Tubbs, R.R., 2013. Mod. Pathol. 26, 1–9.
Shinkai, S., Araki, K., Manabe, O., 1988. J. Chem. Soc., Chem. Commun., 187–189.
Siwy, Z., Trofin, L., Kohli, P., Baker, L.A., Trautmann, C., Martin, C.R., 2005. J. Am. Chem. Soc. 127, 5000–5001.
Sun, Y., Yang, Y.-W., Wu, W., Zhang, S.X.-A., 2012a. Chem. J. Chin. Univ. 33, 1635–1642.
Sun, Y.-L., Yang, B.-J., Zhang, S.X.-A., Yang, Y.-W., 2012b. Chem. Eur. J. 18, 9212–9216.
Wei, A., 2006. Chem. Commun. 37, 1581–1591.
Wei, T., Dong, T., Wang, Z., Bao, J., Tu, W., Dai, Z., 2015. J. Am. Chem. Soc. 137, 8880–8883.
Wessels, J.M., Nothofer, H.-G., Ford, W.E., von Wrochem, F., Scholz, F., Vossmeyer, T., Schroedter, A., Weller, H., Yasuda, A., 2004. J. Am. Chem. Soc. 126, 3349–3356.
Wu, B., Zou, F., Wang, X., Koh, K., Wang, K., Chen, H., 2017. Anal. Methods 9, 2153–2158.
Xianyu, Y., Chen, Y., Jiang, X., 2015. Anal. Chem. 87, 10688–10692.
Yang, Y.-W., 2011. Med. Chem. Commun. 2, 1033–1049.
Yoshikawa, D., Ojima, H., Iwasaki, M., Hiraoka, N., Kosuge, T., Kasai, S., Hirohashi, S., Shibata, T., 2008. Br. J. Cancer 98, 418–425.
Young, S.L., Kellon, J.E., Hutchison, J.E., 2016. J. Am. Chem. Soc. 138, 13975–13984.
Zheng, Y.B., Kiraly, B., Cheunkar, S., Huang, T.J., Weiss, P.S., 2011. Nano Lett. 11, 2061–2065.